Supporting Information

Graphene-sustained Bipolar Covalent Organic Framework for Symmetric Supercapacitors and Capacitive Deionization with Superior Performance

Liming Xu,[a] Yong Liu,[b*] Yuquan Li,[c] Xiaoyang Xuan[d*], Xingtao Xu,[e] Zhiwei Gong [a] and Likun Pan [a*]

[a] *Shanghai Key Laboratory of Magnetic Resonance, School of Physics and Electronic Science, East China Normal University, Shanghai 200241, China*

[b] *School of Materials Science and Engineering, Qingdao University of Science and Technology, Qingdao, Shandong 266042, China*

[c] *College of Environmental Science and Engineering, Yangzhou University, Yangzhou, Jiangsu 225127, China*

[d] *College of Chemistry and Chemical Engineering, Taishan University, Taian, Shandong 271000, China*

[e] *Marine Science and Technology College, Zhejiang Ocean University, Zhoushan, Zhejiang 316022, China*

**Corresponding authors*

Email: lkpan@phy.ecnu.edu.cn (Likun Pan); yong.liu@qust.edu.cn (Yong Liu); xyxuan@tsu.edu.cn (Xiaoyang Xuan)

Materials

Dipyrazino[2,3-f:2',3'-h]quinoxaline-2,3,6,7,10,11-hexacarbonitrile (DQH, 95%) and benzene-1,2,4,5-tetraamine tetrahydrochloride (BA, 97%) were purchased from Bide Pharmatech Ltd. Sodium carbonate (Na_2CO_3, ≥99.8%), sulfuric acid (H_2SO_4, 95.0~98.0%), polyvinylidene fluoride (PVDF, ≥99.5%), 1-methyl-2-pyrrolidone (NMP, ≥99.5%), and sodium chloride (NaCl, ≥99.5%) were purchased from Sinopharm Chemical Reagent Co., Ltd (Shanghai, China). AC (4~7 μm) was purchased from Kuraray (Shanghai) Co., Ltd. All the chemicals were used without further purification.

Structural characterizations

Scanning electron microscopy (SEM) was performed on a Hitachi S-4800 electron microscope. Transmission electron microscopy (TEM) and high-resolution TEM (HR-TEM) images were taken using JEM 2010 JEOL. X-ray diffraction (XRD) patterns of the samples were recorded on a Panalytical PRO PW3040/60 diffractometer at room temperature using Cu-Kα radiation (λ = 1.54056 Å) in the 2θ range of 5~70°. The structure was examined by solid-state ^{13}C NMR with Bruker AVANCE III HD 400MHz. Fourier transform infrared spectra (FT-IR) were recorded in the range 400~4000 cm^{-1} on a Nicolet iS-50 FT-IR spectrometer with KBr pellets. High-resolution XPS spectra were collected using a Thermo ESCALAB 250XI X-ray photoelectron spectroscopy (XPS). N_2 adsorption/desorption tests were performed on an Autosorb iQ analyzer. The pore size distribution was derived from the adsorption branch using the Barret-Joyner-Halenda (BJH) method. The transmittance spectra were recorded by using UV-vis spectrophotometers (Shimadzu UV-3600).

Preparation of working electrode

80 wt.% active material, 10 wt.% Super P (conductive agent) and 10 wt.% polyvinylidene fluoride (binder) were mixed in 1-methyl-2-pyrrolidone to form a homogeneous slurry. Then, the slurry was uniformly cast on graphite substrates (~4 cm^2 for the three-electrode system and ~32 cm^2 for the CDI cell). Finally, the working electrode was dried at 80 °C under vacuum conditions overnight. For the electrochemical and desalination tests, the mass loading of active material on the working electrode was about 4 mg and 60 mg, respectively.

Electrochemical characterizations

Cyclic voltammetry (CV), galvanostatic charge-discharge (GCD), and electrochemical impedance spectroscopy (EIS) tests were conducted using a CHI660E electrochemical analyzer (Shanghai, China) in a 1 M NaCl solution. In the three-electrode system, the Ag/AgCl electrode and

platinum mesh served as reference and counter electrodes, respectively.

Electrochemical calculation

For the three-electrode system, the specific capacitance (C_{S1}, F g^{-1}) of the material was calculated from CV curves according to the following formula:

$$C_{S1} = \frac{\int_{E_1}^{E_2} i(E)d(E)}{2mv(E_2 - E_1)} \quad \text{(S1)}$$

where E_1 and E_2 are the cutoff potentials in CV, i(E) is the instantaneous current, i(E)d(E) is the total voltammetric charge obtained by integration of the positive and negative sweeps in the CV, v is the scan rate, and m is the mass of the individual sample. The specific capacitance (C_{S2}, F g^{-1}) was calculated from the GCD curves according to the following equation:

$$C_{S2} = \frac{I * \Delta t}{m * \Delta V} \quad \text{(S2)}$$

where I, Δt, m, and ΔV, refer to the current (A), discharge time (s), mass of active material (g), and potential window (V), respectively. The areal capacitance (C_{areal}, mF cm^{-2}) was calculated according to the following equation:

$$C_{areal} = \frac{C_{S2} * m}{A} \quad \text{(S3)}$$

where is the area (cm^{-2}) of the electrode.

The relaxation time constant (τ_0, s), real capacitance (Cre(ω), F), imaginary capacitance (Cim(ω), F), diffusion resistance (σ, Ω $s^{-0.5}$), and ion diffusion coefficient (D, cm^2 s^{-1}) were analyzed with EIS based on the following equation:

$$\tau_0 = \frac{1}{f_0} \quad \text{(S4)}$$

$$C(\omega) = C_{re}(\omega) - jC_{im}(\omega) \quad \text{(S5)}$$

$$C_{re}(\omega) = \frac{-Z_{im}}{2\pi f(Z_{re}^2 + Z_{im}^2)} \quad \text{(S6)}$$

$$C_{im}(\omega) = \frac{Z_{re}}{2\pi f(Z_{re}^2 + Z_{im}^2)} \quad (S7)$$

$$Z_{re} = \sigma(2\pi f)^{-0.5} + R_S + R_{ct} \quad (S8)$$

$$D = \frac{R^2T^2}{2A^2C^2n^4F^4\sigma^2} \quad (S9)$$

where f_0, Z_{re}, Z_{im}, f, R_s, R_{ct}, R, T, A, C, n, and F refer to the frequency at 45° phase angle, the real impedance (Ω), the imaginary impedance (Ω), frequency (Hz), ohmic resistance (Ω), charge transfer resistance (Ω), gas constant (8.314 J mol^{-1} K^{-1}), Kelvin temperature (293.15 K), the surface area of the electrode (cm^2), the molar concentration of electrolyte (mol L^{-1}), electron transfer numbers per molecule during electron reaction, and Faraday constant (96,485 C mol^{-1}), respectively.

For the two-electrode system, the gravimetric capacitance (C_{S3}, F g^{-1}) was calculated by the following formula:

$$C_{S3} = \frac{I * \Delta t}{m * \Delta V} \quad (S10)$$

where I, ΔV, Δt, and m, are the discharge current (A), the voltage window (V), the discharge time (s), and the total mass (g) of the active material of two electrodes, respectively. The energy density (E, Wh kg^{-1}) and power density (P, W kg^{-1}) were calculated by the following two equations:

$$E = \frac{C_{S3} * \Delta V^2}{2 * 3.6} \quad (S11)$$

$$P = \frac{3600 * E}{\Delta t} \quad (S12)$$

where C_{S3}, Δt, and ΔV are specific capacitances (F g^{-1}), discharge time (s), and voltage window (V).

Salt removal tests

All salt removal experiments were conducted in a batch-mode CDI system using the constant current mode. A peristaltic pump (volume: 70 mL, flow rate: 100 mL min^{-1}, temperature: room temperature) continuously circulated the NaCl solution through the CDI device. The concentration of the effluent from the pump was recorded in real time by an ion conductivity meter (DDSJ-308A, Precision & Scientific Instrument). The working electrode in the CDI system comprises symmetrical DQHBA or DQHBArGO electrodes separated by a spacer and anion/cation-exchange membrane. The

salt removal experiments were performed in NaCl solutions with various initial concentrations (100, 200, 300, 500, 1000 mg L^{-1}) at ±1.8 V. Additionally, different current densities (100, 200, 300, 400, 500 mA g^{-1}) were tested in a 500 mg L^{-1} NaCl solution. Our previous work established the relationship between the conductivity of NaCl solutions and their concentrations.[1]

Salt removal calculation

The salt removal capacity (SAC, mg g^{-1}), mean desalination rate (MSAR, mg g^{-1} min^{-1}), and charge efficiency (Λ) were defined as follows:

$$SAC = \frac{(C_0 - C_e) * V}{m} \quad \text{(S13)}$$

$$MSAR = \frac{SAC}{t} \quad \text{(S14)}$$

$$\Lambda = \frac{(C_0 - C_e) * V * F}{1000 * M * Q} * 100\% \quad \text{(S15)}$$

where C_0 and C_e are the initial and final NaCl concentrations (mg L^{-1}), V is the volume of NaCl solution (L), m is the mass of the active materials (g), t (s) is the charge time, F is the Faraday constant (96,485 C mol^{-1}), M (58.44 g mol^{-1}) is the relative molar mass of NaCl, and Q (charge, C) is the total charge.

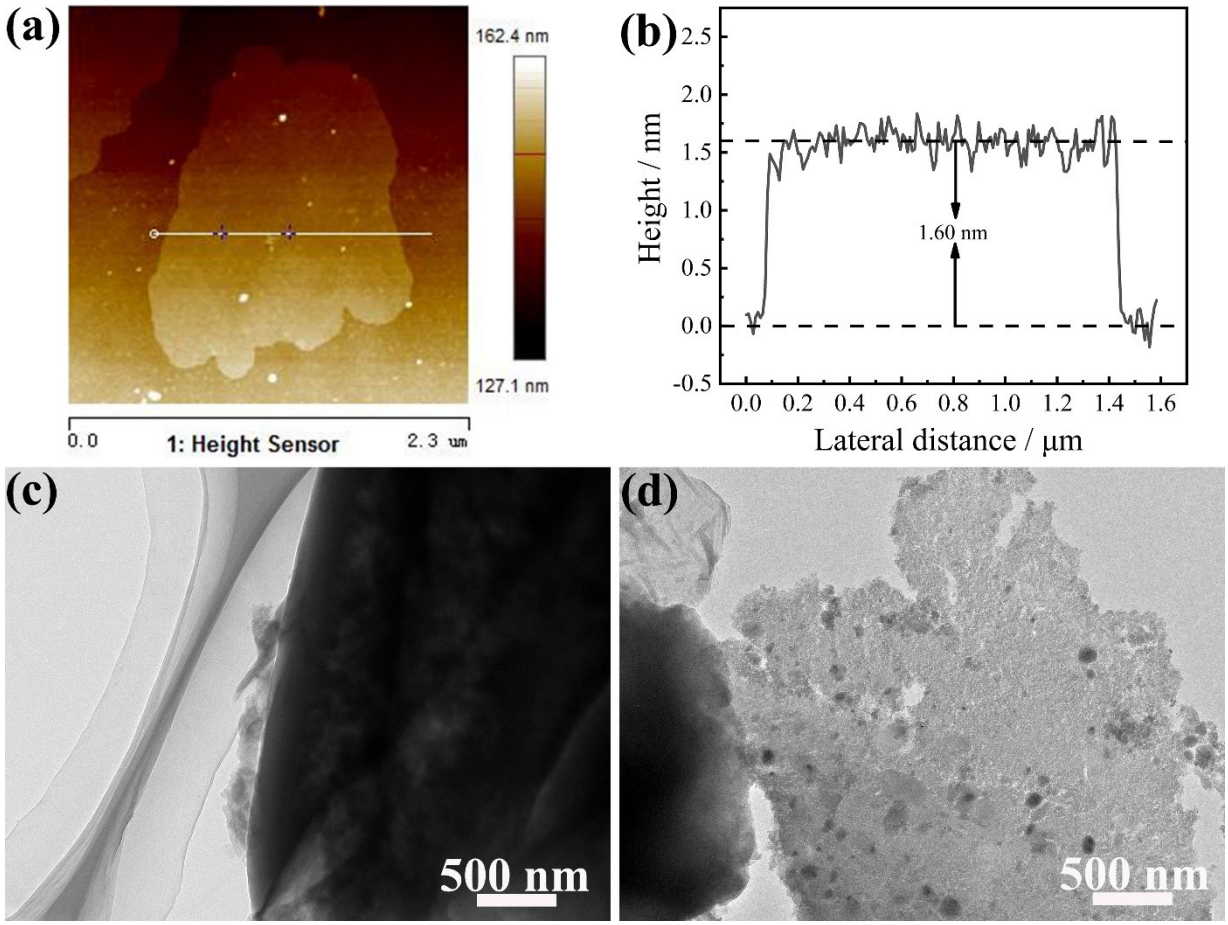

Fig. S1. (a) AFM image and (b) size of GO. TEM images of (c) DQHBA and (d) DQHBArGO-75.

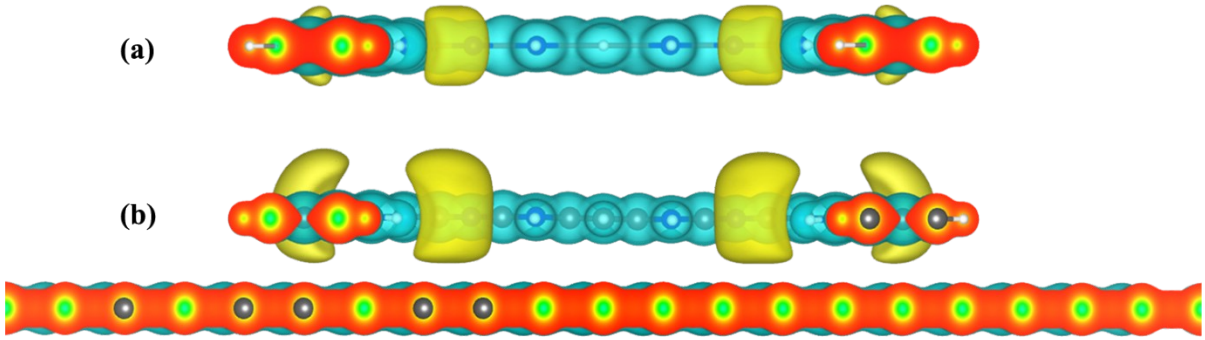

Fig. S2. Parallel views of the deformation charge density image of (a) DQHBA and (b) DQHBArGO-75.

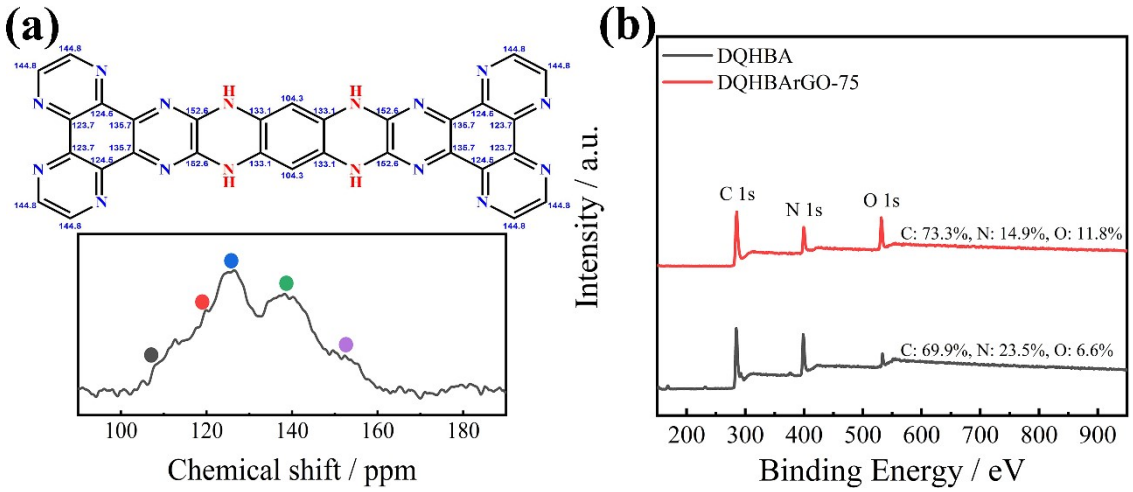

Fig. S3. (a) ^{13}C solid-state NMR of DQHBA. (b) XPS survey spectra of DQHBA and DQHBArGO-75.

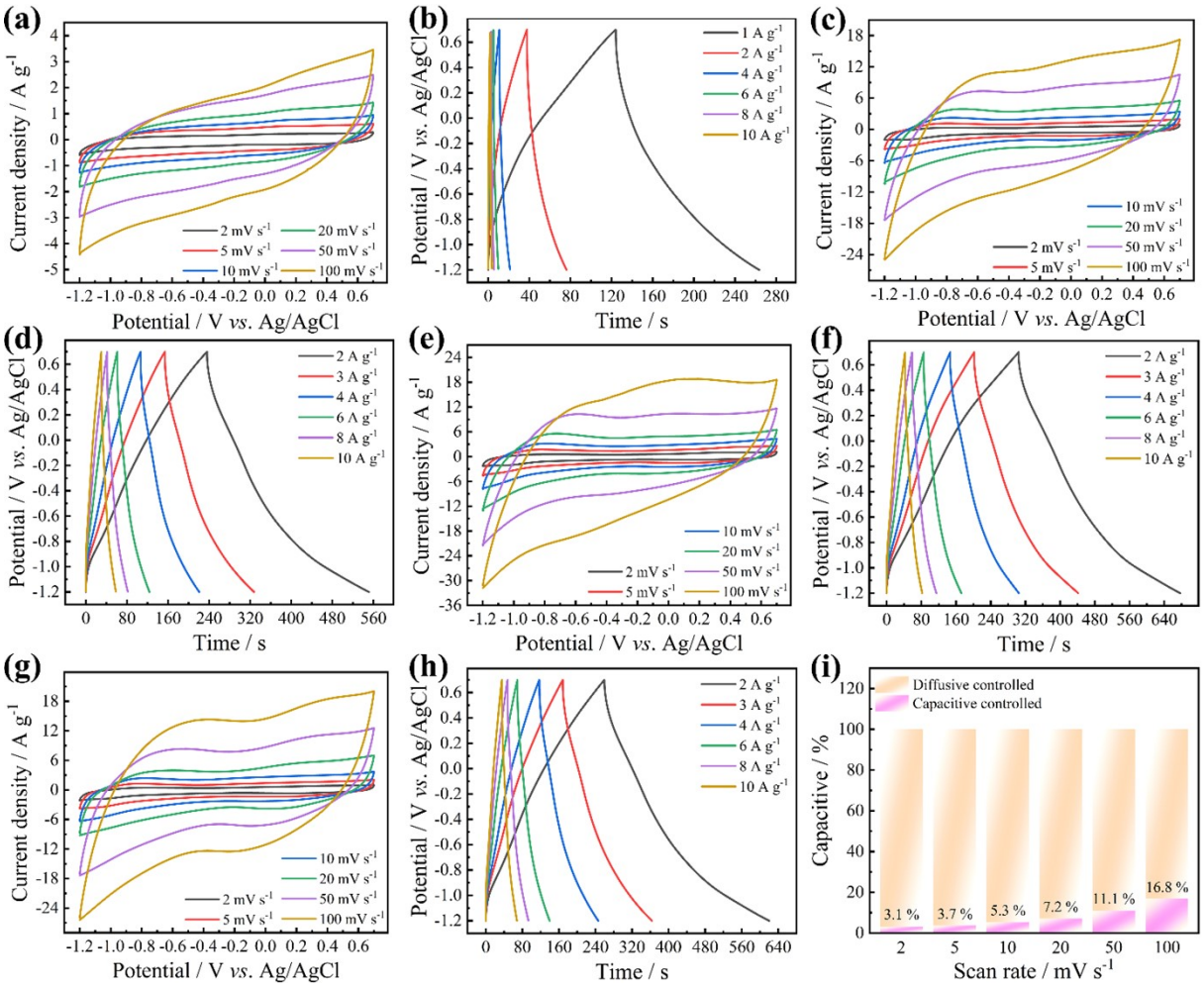

Fig. S4. Electrochemical performances of (a, b) DQHBA, (c, d) DQHBArGO-50, (e, f) DQHBArGO-75, and (g, h) DQHBArGO-100. (i) Percentages of capacitive and diffusion contributions of DQHBA.

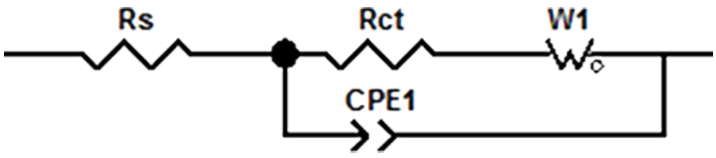

Fig. S5. Equivalent circuit diagram.

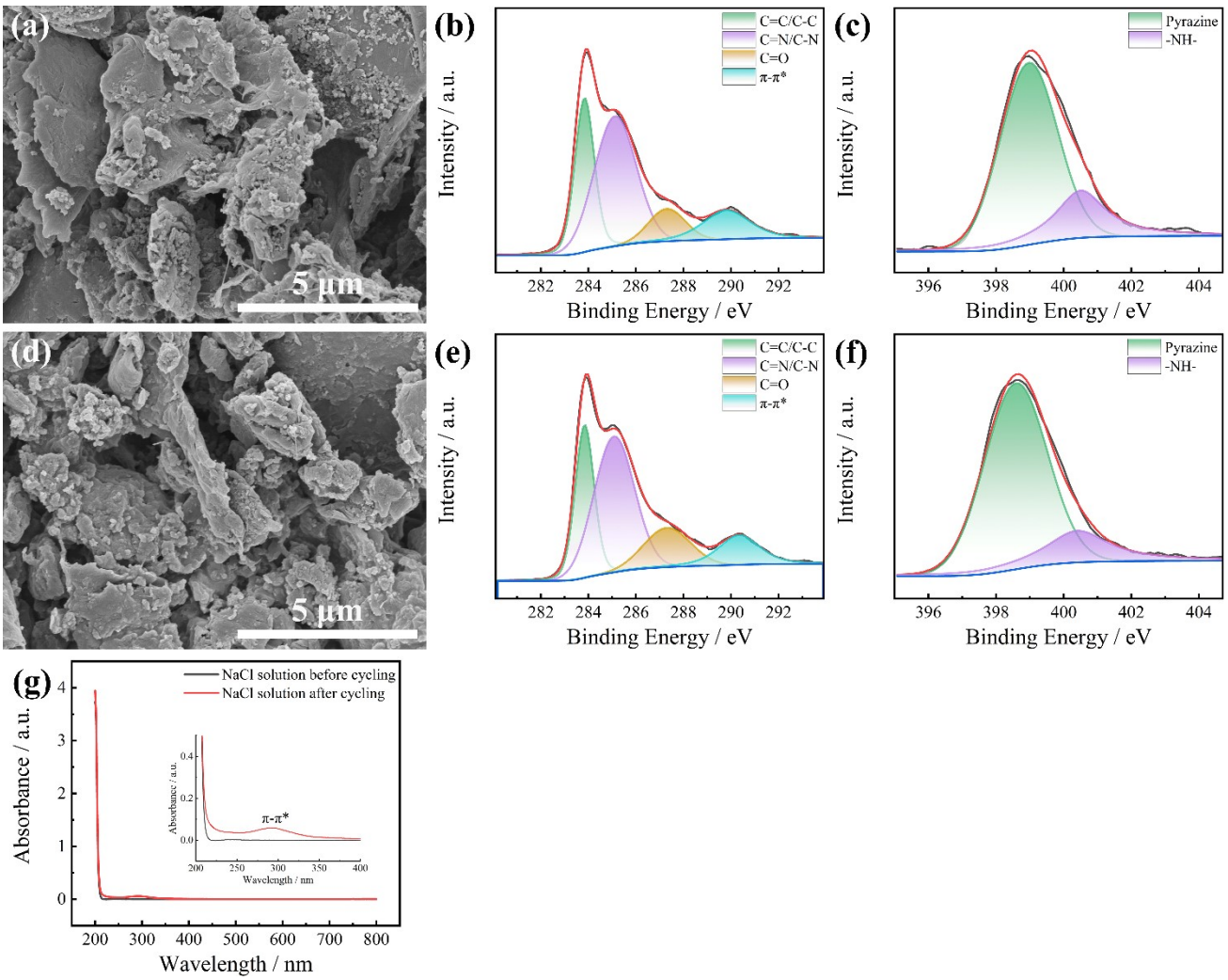

Fig. S6. (a, d) SEM images, high-resolution XPS (b, e) C1s and (c, f) N 1s spectra of the working electrode before and after cycling. (g) The UV-visible absorption spectra of the electrolyte before and after cycling.

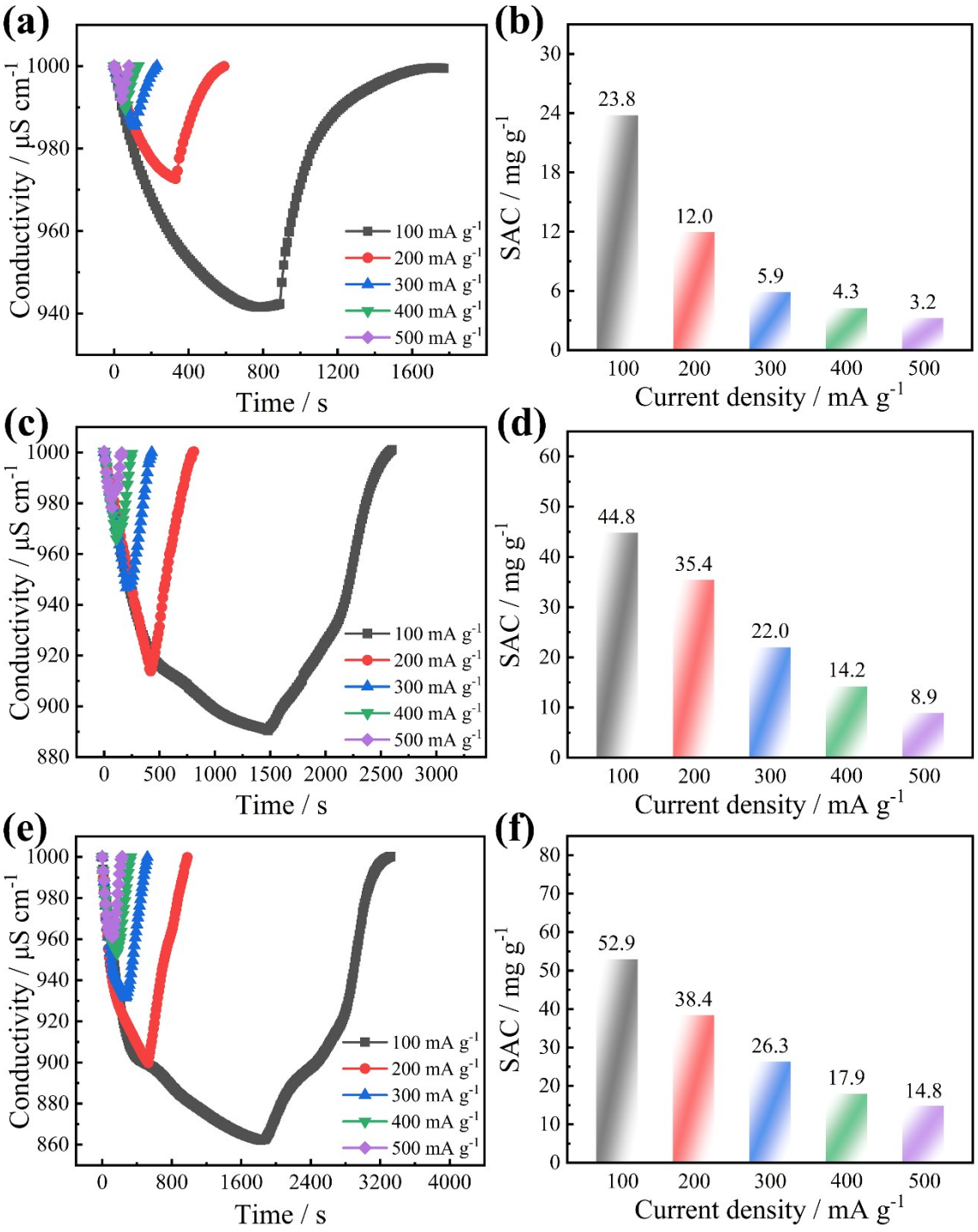

Fig. S7. Conductivity and SAC versus current density of (a, b) DQHBA, (c, d) DQHBArGO-50, and (e, f) DQHBArGO-100.

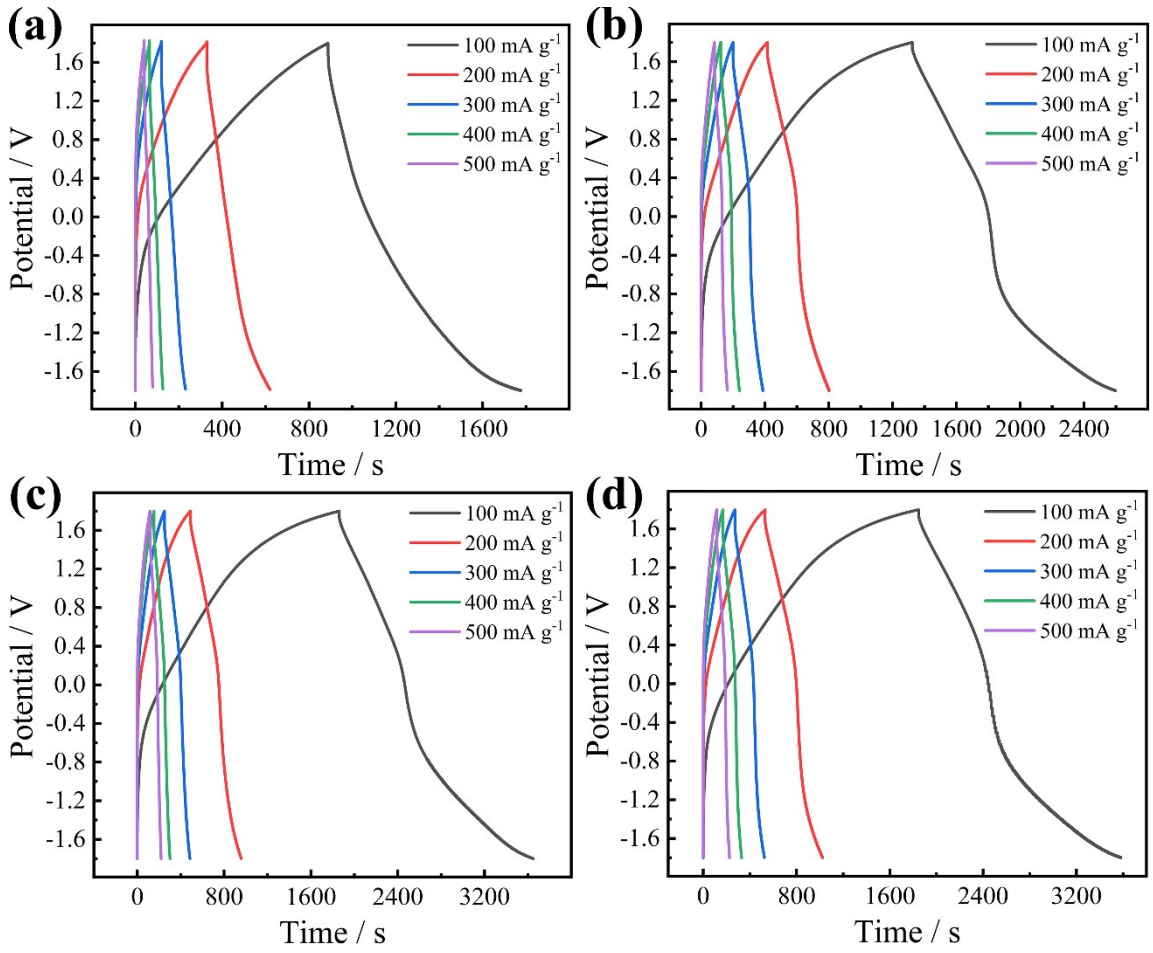

Fig. S8. Voltage response curves of (a) DQHBA, (b) DQHBArGO-50, (c) DQHBArGO-75, and (d) DQHBArGO-100 CDI at various current densities.

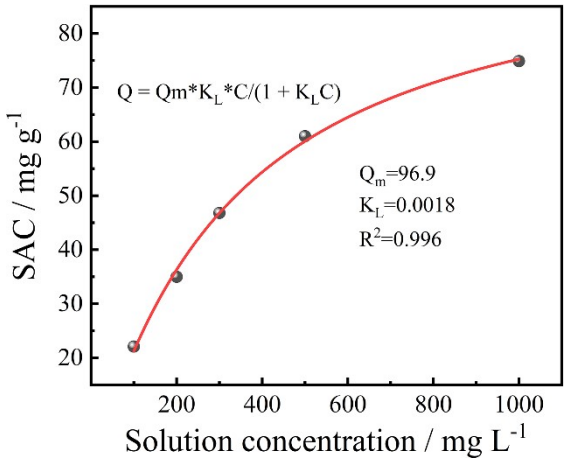

Fig. S9. Desalination capacity of DQHBArGO-75 with different feed concentrations and the corresponding Langmuir isotherm fitted curve.

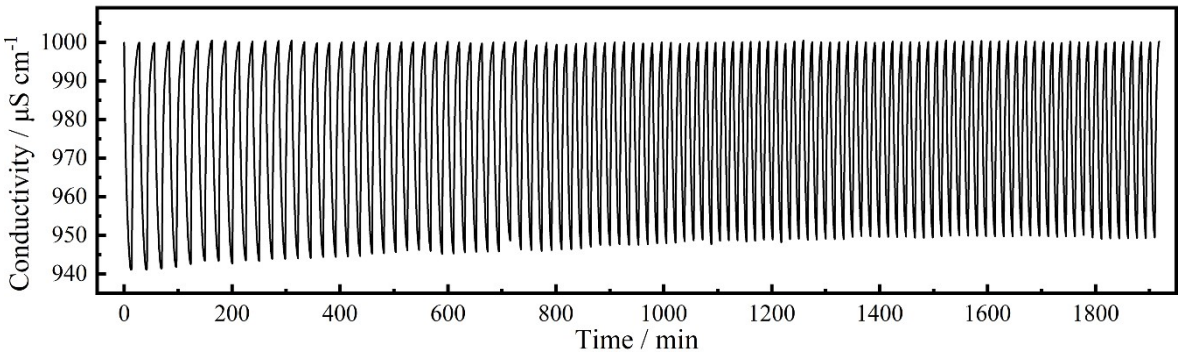

Fig. S10. Cyclic performance of DQHBA.

Table S1. The specific capacitances of DQHBArGO-75 and previously reported polymer-based electrode materials.

Material	Voltage Window /V	Electrolyte	Specific capacitance /F g^{-1}	Ref.
Ni-TAPP/rGO	1.0	6 M KOH	367.5	S2
DPP-TBB-COF	0.5	1 M KOH	384	S3
a-GO@COF-Fs	1.3	1 M H_2SO_4	295	S4
Arylamine-Linked 2D COF	1.1	1 M H_2SO_4	271	S5
Triphenylamine-based COF	1.0	1 M H_2SO_4	263.1	S6
$Ti_3C_2T_x$ MXene-polydopamine	1.5	1 M NaCl	112	S7
Dimethoxybenzene-dithiophene-based COF	1.0	1 M KOH	273.3	S8
TpPa-$(OH)_2$/rGO	0.8	1 M H_2SO_4	371.1	S9
Tetrathiafulvalene-based COF	3.5	$EMIMBF_4$	130	S10
COF/MXene	0.7	2 M HCl	390	S11
Carbon-based elastic foams supported COF	1.0	1 M H_2SO_4	129.2	S12
Triazine-based COF	2.0	0.5 M K_2SO_4	182.6	S13
DAAQ-COFs/GA	1.0	1 M H_2SO_4	378	S14
v-COF-GAs	0.8	1 M H_2SO_4	289	S15
rGO/COF-20	1.0	1 M H_2SO_4	321	S16
DQHBArGO-75	1.9	1 M NaCl	397.9	**This work**

Table S2. Diffusion resistance and Na^+ and Cl^- diffusion coefficient of DQHBA, DQHBArGO-50, DQHBArGO-75, and DQHBArGO-100 during the electrochemical process.

Material	Diffusion resistance /Ω $s^{-0.5}$	Na^+ diffusion coefficient (cm^2 s^{-1})	Cl^- diffusion coefficient (cm^2 s^{-1})
DQHBA	17.88	$8.27*10^{-14}$	$2.62*10^{-14}$
DQHBArGO-50	3.24	$2.00*10^{-12}$	$6.33*10^{-13}$
DQHBArGO-75	1.60	$1.03*10^{-11}$	$3.26*10^{-12}$
DQHBArGO-100	2.26	$5.22*10^{-12}$	$1.65*10^{-12}$

References

1. H.B. Li, T. Lu, L.K. Pan, Y.P. Zhang, Z. Sun, *J. Mater. Chem.*, 2009, **19**, 6773-6779.
2. A.Q. Zhang, P. Ran, X. Han, S.W. Ke, A.Q. Qiu,. Z.D. Zhang, Y. Lv, M.N. Ding, J.L. Zuo, *J. Mater. Chem. A,* 2024, **12**, 22037-22044.
3. L. Luo, C.B. Li, Y.C. Wang, P.Y. Chen, Z.Q. Zhou, T.W. Chen, K.L. Wu, S.Y. Ding, L.X. Tan, J.G. Wang, X.F. Shao, Z.T. Liu, *Small*, 2024, **20**, 2402993.
4. D. Cui, W. Xie, S.R. Zhang, Y.H. Xu, Z.M. Su, *Polym. Chem.*, 2023, **14**, 803-810.
5. Z.F. Yang, J.J. Liu, Y.S. Li, G. Zhang, G.L. Xing, L. Chen, *Angew. Chem. Int. Ed.*, 2021, **60**, 20754-20759.
6. S.X. Xiong, J. Liu, Y.C. Wang, X.Q. Wang, J. Chu, R.L. Zhang, M. Gong, B.H. Wu, *J. Appl. Polym. Sci.*, 2022, **139**, e51510.
7. Q. Li, X.T. Xu, J.R. Guo, J.P. Hill, H.S. Xu, L.X. Xiang, C. Li, Y. Yamauchi, Y.Y. Mai, *Angew. Chem. Int. Ed.*, 2021, **60**, 26528-26534.
8. S. Li, B. Kumbhakar, B. Mishra, J. Roeser, N. Chaoui, J. Schmidt, A. Thomas, P. Pachfule, *ACS Appl. Energy Mater.*, 2023, **6**, 9256-9263.
9. D.P. Hu, Y.H. Jia, S.P. Yang, C.Q. Lin, F.Y. Huang, R.H. Wu, S.M. Guo, K.F. Xie, P.C. Du, *Chem. Eng. J.*, 2024, **488**, 151160.
10. A. Chatterjee, J.M. Sun, K.S. Rawat, V.V. Speybroeck, P.V.D. Voort, *Small*, 2023, **19**, 2303189.
11. N. An, Z. Guo, C. Guo, M.Q. Wei, D.M. Sun, Y.Y. He, W.L. Li, L. Zhou, Z.G. Hu, X.Y. Dong, *Chem. Eng. J.*, 2023, **458**, 141434.
12. Y.Y. Dong , Y.L. Wang, X.F. Zhang, Q. Lai, Y.K. Yang, *Chem. Eng. J.*, 2022, **449**, 137858.
13. Y. Kumar, I. Ahmad, A. Rawat, R.K. Pandey, P. Mohanty, R. Pandey, *ACS Appl. Mater. Interfaces*, 2024, **16**, 11605-11616.
14. N. An, Z. Guo, J. Xin, Y.Y. He, K.F. Xie, D.M. Sun, X.Y. Dong, Z.G. Hu, *J. Mater. Chem. A*, 2021, **9**, 16824-16833.
15. Y.Q. Jiang, Z.Y. Zhang, D. Chen, J.G. Du, Y.H. Yang, S. Wang, F. Guo, X.Y. Chen, C. Gao, W.J. Wang, P.W. Liu, *Adv. Mater.*, 2022, **34**, 2204250.
16. C.J. Wang, F. Liu, J.S. Chen, Z.W. Yuan, C. Liu, X.S. Zhang, M.Y. Xu, L. Wei, Y. Chen, *Energy Storage Mater.*, 2020, **32**, 448-457.